Velocity-space substructures and bar resonances in an N-body Milky Way

Asano, T.; Fujii, M.S.; Baba, J.; Bédorf, J.; Sellentin, E.; Portegies Zwart, S.F.; ... ; Boily, C.

The Predictive Power of Computational Astrophysics as a Discovery Tool
Proceedings IAU Symposium No. 362, 2023
D. Bisikalo, D. Wiebe & C. Boily, eds.
doi:10.1017/S1743921322001521

Velocity-space substructures and bar resonances in an N-body Milky Way

Tetsuro Asano[1]†, Michiko S. Fujii[1], Junich Baba[2], Jeroen Bédorf[3,5], Elena Sellentin[3,4] and Simon Portegies Zwart[3]

[1]Department of Astronomy, Graduate School of Science, The University of Tokyo, 7-3-1 Hongo, Bunkyo-ku, Tokyo 113-0033, Japan

[2]National Astronomical Observatory of Japan, Mitaka-shi, Tokyo 181-8588, Japan

[3]Leiden Observatory, Leiden University, NL-2300RA Leiden, The Netherlands

[4]Mathematical Institute, Leiden University, NL-2300RA Leiden, The Netherlands

[5]Minds.ai, Inc., Santa Cruz, the United States

Abstract. The velocity-space distribution of the solar neighborhood stars shows complex substructures (moving groups) including the well-known Hercules stream. Recently, the Gaia observation revealed their detailed structures, but their origins are still in debate. We analyzed a high-resolution N-body simulation of a Milky Way (MW)-like galaxy. To find velocity-space distributions similar to that of the solar neighborhood stars, we used Kullback-Leibler divergence (KLD), which is a metric to measure similarities between probability distributions. The KLD analysis shows the time evolution and the spatial variation of the velocity-space distribution. Velocity-space distributions with small KLDs (i.e. high similarities) are frequently but not always detected around $(R, \phi) = (8.2\,\mathrm{kpc}, 30^\circ)$ in the simulated MW. In the velocity-map with smallest KLD, the velocity-space substructures are made from bar resonances.

Keywords. Galaxy: disk, Galaxy: kinematics and dynamics, (Galaxy:) solar neighborhood, Galaxy: structure, methods: numerical

1. Introduction

The *Gaia* (Gaia Collaboration *et al.* 2016) observation has revealed the detailed phase-space distribution of the stars in the Milky Way (MW). Fig. 1 shows the velocity-space distribution of the solar neighbor stars observed in the *Gaia* Early Data Release 3 (EDR3; Gaia Collaboration *et al.* 2021). The names and the locations of the major substructures are indicated in the figure. The most prominent substructure is the Hercules stream. Dehnen (2000) demonstrated that the Hercules stream can be explained by trapping in the 2:1 outer Lindblad resonance (OLR) of the bar using test particle simulations. This model requires the fast rotating bar with the pattern speed of $\Omega_\mathrm{b} \gtrsim 50\,\mathrm{km\,s^{-1}\,kpc^{-1}}$, but the recent pattern speed measurements of the MW's bar suggest the slower bar of $\Omega_\mathrm{b} \lesssim 40\,\mathrm{km\,s^{-1}\,kpc^{-1}}$ (e.g. Bovy *et al.* 2019; Clarke *et al.* 2019; Sanders *et al.* 2019).

In the case of the slow bar, trapping in the corotation resonance (CR) well explains the structures of the Hercules stream (e.g. Pérez-Villegas *et al.* 2017; Binney 2020; Chiba *et al.* 2021). Higher order resonances are also the candidates for the origins of the Hercules stream and the other substructures (e.g. Hunt & Bovy 2018; Hattori *et al.* 2019; Monari *et al.* 2019; Kawata *et al.* 2021; Trick *et al.* 2021). Some studies suggested

† email: t.asano@astron.s.u-tokyo.ac.jp

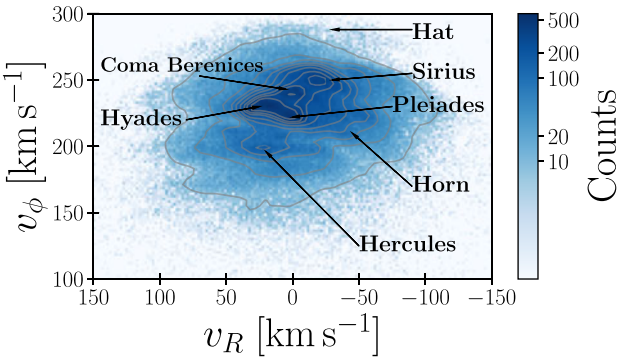

Figure 1. Solar neighbourhood star distribution in radial velocity versus azimuthal velocity (v_R-v_ϕ) space.

that the velocity-space substructures originate from the spiral arms (e.g. Hunt *et al.* 2019; Khoperskov *et al.* 2021) or external perturbations by the satellite galaxies (e.g. Laporte *et al.* 2019; Hunt *et al.* 2021).

Most of the previous studies use the test particle simulations. They assume static and symmetric gravitational potentials. Note that Chiba *et al.* (2021) analytically modeled the influences of the bar's slowing down.

Asano *et al.* (2020) used an N-body MW model simulated by Fujii *et al.* (2019) and found a Hercules-like stream made from 4:1 OLR and 5:1 OLR. This study confirmed that bar resonances form velocity-space substructures even in the non-static N-body models. We analyze the same simulation data but put the focus on the time evolution and the spatial variation of the velocity-space distribution. To evaluate the similarity of the velocity-space distribution in the simulation and that in the *Gaia* observation, we use the Kullback-Leibler divergence.

2. Methods

We analyzed the model MWaB, which is one of the N-body models simulated by Fujii *et al.* (2019). The numbers of the bulge, disk, and dark-matter halo particles are 30M, 208M, and 4.9B, respectively. The simulations were performed using the parallel GPU tree-code, `BONSAI` (Bédorf *et al.* 2012; Bédorf *et al.* 2014). Fig. 2 shows the face-on view of the model at $t = 10$ Gyr. Fig. 3 shows the bar's pattern speed and the bar's strength as functions of time. We determined them using the Fourier decomposition:

$$\frac{\Sigma(R,\phi)}{\Sigma_0(R)} = \sum_{m=0}^{\infty} A_m(R)\exp\{im[\phi-\phi_m(R)]\}, \tag{2.1}$$

where $\Sigma(R,\phi)/\Sigma_0(R)$ is the disk surface density normalized at each radius. The bar pattern speed (Ω_b) and the strength are the rate of change of $\phi_2(R<3\,\mathrm{kpc})$ and A_2, respectively. For details, see Fujii *et al.* (2019) and Asano *et al.* (2020).

We use Kullback-Leibler divergence (KLD) to quantitatively evaluate the similarities between the velocity-space distributions in the simulation and that in the *Gaia* EDR3 observation. To compute the KLD, we first determine a probability distribution in the velocity space for the stars within 200 pc from the Sun. We divide the $\hat{v}_R$ versus $\hat{v}_\phi$ space in a range of $(-0.5, 0.5)\times(-0.333, 0.333)$ into 48×32 cells, where the $\hat{v}_R$ and $\hat{v}_\phi$ are the relative velocities defined as $\hat{v}_R \equiv (v_R-\bar{v}_R)/\bar{v}_\phi$ and $\hat{v}_\phi \equiv (v_\phi-\bar{v}_\phi)/\bar{v}_\phi$, respectively. The mean velocities $(\bar{v}_R, \bar{v}_\phi)$ are determined for the stars within 200 pc from the Sun. We obtain the probability of which we find a star in the i-th cell, p_i, diving the number of the stars in the cell by the total number of the stars. We also determine the counterpart

https://doi.org/10.1017/S1743921322001521 Published online by Cambridge University Press

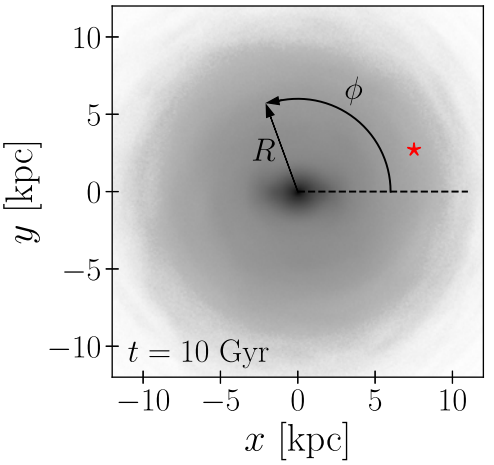

Figure 2. Faceon view of the N-body model. The star indicates the position of $(R, \phi) = (8\,\mathrm{kpc}, 20^\circ)$.

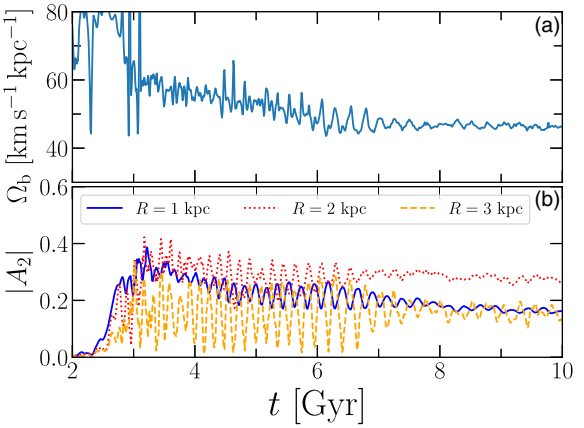

Figure 3. (a) Time evolution of the bar's pattern speed. (b) Time evolution of the bar's strength $|A_2|$ at $R = 1$, 2, and 3 kpc.

of p in the N-body model, q, which is evaluated at the 648 points of

$$\begin{cases} R = (6 + 0.5i)\,\mathrm{kpc} & (i = 0, \ldots, 8), \\ \phi = (-180 + 5j)^\circ & (j = 0, \ldots, 71), \\ z = 0\,\mathrm{kpc}, \end{cases} \tag{2.2}$$

in each snapshot. The KLD between p and q is defined by

$$\mathrm{KLD}(p||q) = \sum_{i=1}^{N} p_i \log \frac{p_i}{q_i}. \tag{2.3}$$

It is a quantity like 'distance' between p and q since it satisfies (i) $\mathrm{KLD}(p||q) \geq 0$ and (ii) $\mathrm{KLD}(p||q) = 0$ if and only if p and q are identical. Therefore, The smaller the KLD is, the more q is similar to p.

https://doi.org/10.1017/S1743921322001521 Published online by Cambridge University Press

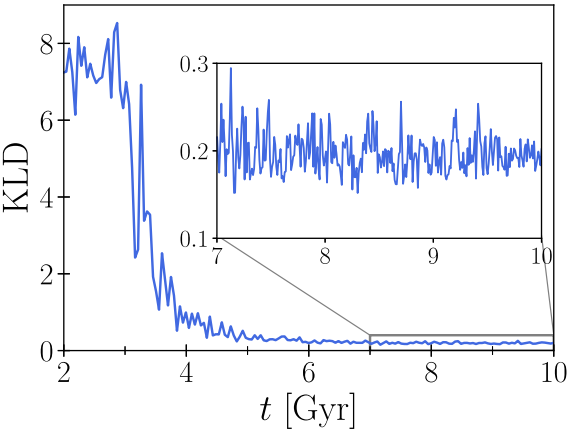

Figure 4. Time evolution of the KLD of the velocity-space distribution at $(R, \phi) = (8\,\mathrm{kpc}, 20^\circ)$.

3. Results

3.1. *Time evolution of the velocity-space distribution*

Fig. 4 shows the KLD of the velocity-space distribution at $(R, \phi) = (8\,\mathrm{kpc}, 20^\circ)$ as a functions of time. We select this position as a reference point because Asano *et al.* (2020) found a Hercules-like stream by eyes in the final snapshot ($t = 10\,\mathrm{Gyr}$). The KLD is smaller in the later epochs of the simulation than in the earlier epochs. This is because Fujii *et al.* (2019) adjusted the initial parameters of the model so that the disk and bulge properties at the end of the simulation well reproduce the observed ones. The KLD drops rapidly at $t \simeq 3\,\mathrm{Gyr}$, at which a clear bar structure appears. From $t \simeq 3\,\mathrm{Gyr}$ to $t \simeq 7\,\mathrm{Gyr}$, the KLD decreases as the bar's pattern speed slows down. The correlation of the KLD and the bar evolutions indicates that bar affects the velocity-space stellar distribution. The KLD oscillates after $t \simeq 7\,\mathrm{Gyr}$, which means the velocity-space distribution at $(R, \phi) = (8\,\mathrm{kpc}, 20^\circ)$ is not always similar to that of the solar neighborhood.

3.2. *Spatial variation of the velocity-space distribution*

In this section, we investigate where in the disk we frequently detect velocity-space distributions similar to that of the solar neighborhood. We define that a velocity-space distribution is similar to that of the solar neighborhood if its KLD is less than 0.2, which is the KLD of the velocity-space distribution at $(R, \phi) = (8, \mathrm{kpc}, 20^\circ)$ at $t = 10\,\mathrm{Gyr}$. Here, we analyzed the snapshots after $t = 7\,\mathrm{Gyr}$. The panel (a) in Fig. 5 shows how many times the velocity-space distributions with KLD < 0.2 are detected at each angle with respect to the bar. The bar's major axis is aligned with the x-axis. We map the angles of $\phi < 0$ to $\phi + 180^\circ$ in the figure since we focus only on the relative angles with respect to the major axis. The numbers of the detections of the small KLDs at $R = 7.5$ and 9 kpc are more than four times smaller than those at $R = 8$, 8.2, and 8.5 kpc. The peaks of the histograms differ by R. The peak moves in the positive direction of ϕ as R increases. The histogram at $R = 8.2\,\mathrm{kpc}$, which is the distance between the Sun and the Galactic center, has a peak at $\phi \simeq 30^\circ$. This angle matches the observationally estimated bar angle (Bland-Hawthorn & Gerhard 2016). The R and ϕ dependence of the KLD indicates that bar resonances impact the velocity-space space distribution because the spacial distribution of the resonantly trapped stars is also dependent on R and ϕ (e.g. Ceverino & Klypin 2007; Khoperskov *et al.* 2020).

https://doi.org/10.1017/S1743921322001521 Published online by Cambridge University Press

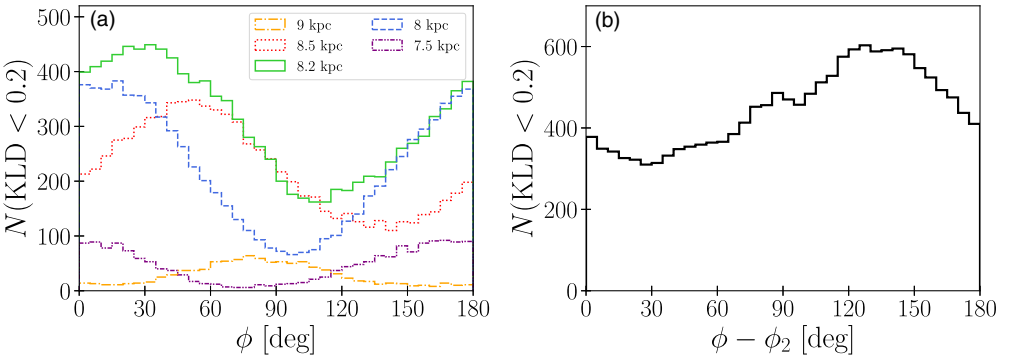

Figure 5. Histograms of the angles at which the KLD is less then 0.2. (a) The angle with respect to the bar. The yellow, red, green, blue, and purple lines shows the histograms at $R = 9$, 8.5, 8.2, 8, and 7.5 kpc, respectively. (b) The angle with respect to the spiral arms.

The panel (b) in Fig. 5 shows the histogram of the angles as the panel (a) but with respect to the spirals ($\phi - \phi_2$). We define the spiral position as a phase angle of the Fourier $m = 2$ mode $\phi_2(R)$. Here, we limit the analysis at $R = 8$ and 8.5 kpc. The histogram shows the peak at $\phi - \phi_2 \simeq 130°$. This is the inter-arm region since the position of spiral arms are $\phi - \phi_2 = 0°$ and 180°. This is consistent with the observations of the spiral arms of the MW. The Sun locates in the inter-arm regions of the MW's spiral arms such as Perseus and Sagittarius-Carina (Reid *et al.* 2019). We note that the Sun is close to the 'Local arm', but that it is relatively weak.

The fluctuation of the KLD seen in Fig. 4 may be due to the spiral arms. Dynamic transient spiral arms efficiently cause the radial migrations of stars (e.g. Baba *et al.* 2013). Spiral arms may make the stars escape from the bar resonances and weaken the bar's underlying impacts on the velocity-space distribution.

4. Summary

We have evaluated the similarities between the velocity-space distributions in the simulation and that in the observation of the solar neighborhood stars using the KLD. We have obtained the following results.

(a) The time evolution of the KLD is linked with the bar's evolution. The KLD at $(R, \phi) = (8\,\mathrm{kpc}, 20°)$ drops rapidly at the bar formation epoch. It decreases while the bar is decelerating.
(b) The KLD fluctuates even after the bar's slowdown, which indicates that the velocity-space distribution at $(R, \phi) = (8\,\mathrm{kpc}, 20°)$ is not always similar to that of the solar neighborhood stars.
(c) The detection counts of the velocity-space distributions with small KLDs are strongly dependent on R and ϕ. One of the positions where the small KLDs are most frequently detected is $(R, \phi) = (8.2\,\mathrm{kpc}, 30°)$, which matches the Sun's position in the MW.
(d) The detection frequency is higher in the inter-arm regions than the arm regions.

These results indicate that the bar resonances have significant impact on the velocity-space distribution even though the gravitational potential is not static. In Asano *et al.* (2021) we see that bar resonances form the substructures in the velocity-space distributions with small KLDs.

https://doi.org/10.1017/S1743921322001521 Published online by Cambridge University Press

References

Asano, T., Fujii, M. S., Baba, J., Bédorf, J., Sellentin, E., Portegies Zwart, S., 2020, *MNRAS* 499, 2416

Asano, T., Fujii, M. S., Baba, J., Bédorf, J., Sellentin, E., Portegies Zwart, S., 2021, arXiv e-prints, arXiv:2112.00765

Baba, J., Saitoh, T. R., Wada, K., 2013, *ApJ* 763, 46

Bédorf, J., Gaburov, E., Portegies Zwart, S., 2012, *Journal of Computational Physics* 231, 2825

Bédorf, J., Gaburov, E., Fujii, M. S., Nitadori, K., Ishiyama, T., Portegies Zwart, S., 2014, in *International Conference for High Performance Computing, Networking, Storage and Analysis*, Proc. SC'14, p. 54

Binney, J., 2020, *MNRAS* 495, 895

Bland-Hawthorn, J., Gerhard, O., 2016, *ARAA* 54, 529

Bovy, J., Leung, H. W., Hunt, J. A. S., Mackereth,J. T., García-Hernández, D. A., Roman-Lopes, A., 2019, *MNRAS* 490, 4740

Ceverino, D., Klypin, A., 2007, *MNRAS* 379, 1155

Chiba, R., Friske, J. K. S., Schönrich, R., 2021, *MNRAS* 500, 4710

Clarke, J. P., Wegg, C., Gerhard, O., Smith, L. C., Lucas, P. W., Wylie S. M., 2019, *MNRAS* 489, 3519

Dehnen, W., 2000, *AJ* 119, 800

Fujii, M. S., Bédorf, J., Baba, J., Portegies Zwart, S., 2019, *MNRAS* 482, 1983

Gaia Collaboration *et al.* 2016, *A&A* 595, A1

Gaia Collaboration *et al.* 2018, *A&A* 616, A11

Gaia Collaboration *et al.* 2021, *A&A* 649, A1

Hattori, K., Gouda, N., Tagawa, H., Sakai, N., Yano, T., Baba, J., Kumamoto, J., 2019, *MNRAS* 484, 4540

Hunt, J. A. S., Bovy, J., 2018, *MNRAS* 477, 3945

Hunt, J. A. S., Bub, M. W., Bovy, J., Mackereth, J. T., Trick, W. H., Kawata, D., 2019, *MNRAS* 490, 1026

Hunt, J. A. S., Stelea, I. A., Johnston, K. V., Gandhi, S. S., Laporte, C. F. P., Bédorf, J, 2021, *MNRAS* 508, 1459

Kawata, D., Baba, J., Hunt, J. A. S., Schönrich, R., Ciucă, I., Friske, J., Seabroke, G., Cropper, M., 2021, *MNRAS* 508, 728

Khoperskov, S., Gerhard, O., Di Matteo, P., Haywood, M., Katz, D., Khrapov, S., Khoperskov, A., Arnaboldi, M., 2020, *A&A* 634, L8

Khoperskov, S., Gerhard, O., 2021, arXiv e-prints, arXiv:2111.15211

Laporte, C. F. P., Minchev, I., Johnston, K. V., Gómez, F. A., 2019, *MNRAS* 485, 3134

Monari, G., Famaey, B., Siebert, A., Wegg, C., Gerhard, O., 2019, *A&A* 626, A41

Pérez-Villegas, A., Portail, M., Wegg, C, Gerhard, O., 2017, *ApJ* 840, L2

Reid, M. J., *et al.*, 2019, *ApJ* 885, 131

Sanders, J. L., Smith, L., Evans, N. W., 2019, *MNRAS* 488, 4552

Trick, W. H., Fragkoudi, F., Hunt, J. A. S., Mackereth, J. T., White, S. D. M., 2021, *MNRAS* 500, 2645

https://doi.org/10.1017/S1743921322001521 Published online by Cambridge University Press